



Experimental investigation of frictional melting of argillite at high slip rates: Implications for seismic slip in subduction-accretion complexes

Kohtaro Ujiie,^{1,2} Akito Tsutsumi,³ Yuri Fialko,² and Haruka Yamaguchi⁴

Received 20 October 2008; revised 23 January 2009; accepted 2 March 2009; published 30 April 2009.

[1] Discovery of pseudotachylytes from exhumed accretionary complexes indicates that frictional melting occurred along illite-rich, argillite-derived slip zones during subduction earthquakes. We conducted high-velocity friction experiments on argillite at a slip rate of 1.13 m/s and normal stresses of 2.67–13.33 MPa. Experiments show slip weakening followed by slip strengthening. Slip weakening is associated with the formation and shearing of low-viscosity melt patches. The subsequent slip strengthening occurred despite the reduction in shear strain rate due to the growth (thickening) of melt layer, suggesting that the viscosity of melt layer increased with slip. Microstructural and chemical analyses suggest that the viscosity increase during the slip strengthening is not due to an increase in the volume fraction of solid grains and bubbles in the melt layer but could be caused primarily by dehydration of the melt layer. Our experimental results suggest that viscous braking can be efficient at shallow depths of subduction-accretion complexes if substantial melt dehydration occurs on a timescale of seismic slip. Melt lubrication can possibly occur at greater depths within subduction-accretion complexes because the ratio of viscous shear to normal stress decreases with depth. Argillite-derived natural pseudotachylytes formed at seismogenic depths in subduction-accretion complexes are more hydrous than the experimentally generated pseudotachylytes and may be evidence of nearly complete stress drop.

Citation: Ujiie, K., A. Tsutsumi, Y. Fialko, and H. Yamaguchi (2009), Experimental investigation of frictional melting of argillite at high slip rates: Implications for seismic slip in subduction-accretion complexes, *J. Geophys. Res.*, *114*, B04308, doi:10.1029/2008JB006165.

1. Introduction

[2] Most of the world's largest earthquakes occur along convergent plate boundaries [*Pacheco et al.*, 1993; *Scholz*, 2002]. Theoretical studies and detailed seismic reflection surveys suggest that during great earthquakes, such as the 1944 Tonankai earthquake (moment magnitude 8.1) at the Nankai accretionary margin, subduction thrust ruptures tend to propagate along splay faults (or out-of-sequence thrusts) that rise from the subduction interface [*Park et al.*, 2002; *Kame et al.*, 2003; *Moore et al.*, 2007]. Exhumed subduction-accretion complexes provide a unique opportunity to investigate conditions in seismogenic zones. Pseudotachylytes (i.e., solidified frictional melts) were recently found in

exhumed subduction thrusts, roof thrusts of duplex structures [*Ikesawa et al.*, 2003; *Rowe et al.*, 2005; *Ujiie et al.*, 2007] and out-of-sequence thrusts [*Mukoyoshi et al.*, 2006; *Okamoto et al.*, 2006]. They were formed at depths of 2.5–14 km. Pseudotachylytes from exhumed accretionary complexes are direct evidence that at least some seismic slip along subduction thrusts and out-of-sequence thrusts resulted in frictional melting. In subduction-accretion complexes, pseudotachylyte-bearing faults primarily occur in argillite that commonly constitutes the matrix of tectonic mélange. Field and laboratory studies suggest that pseudotachylytes were formed by frictional melting of illite-rich slip zone at ~1100°C [*Ujiie et al.*, 2007]. Therefore insights into the dynamic shear strength of illite-rich argillite during frictional melting are important for understanding of seismic slip in subduction-accretion complexes.

[3] Melting of crystalline rocks such as gabbro and tonalite has been studied in several high-velocity (order of m/s) rock-friction experiments (HVRFE) [*Tsutsumi and Shimamoto*, 1997; *Hirose and Shimamoto*, 2005; *Di Toro et al.*, 2006a, 2006b]. These experimental data show a complex evolution of shear stresses prior to and after the onset of melting, and explained by coupled thermal-fluid-mechanical models [*Fialko and Khazan*, 2005; *Sirono et al.*, 2006; *Nielsen et al.*, 2008]. *Tsutsumi and Shimamoto* [1997] and *Hirose and Shimamoto* [2005] reported a typical evolution of apparent friction of gabbro during HVRFE:

¹Institute for Research on Earth Evolution, Japan Agency for Marine-Earth Science and Technology, Yokohama, Kanagawa, Japan.

²Institute of Geophysics and Planetary Physics, Scripps Institution of Oceanography, University of California, San Diego, La Jolla, California, USA.

³Department of Geology and Mineralogy, Division of Earth and Planetary Sciences, Graduate School of Science, Kyoto University, Kyoto, Japan.

⁴Institute for Study of the Earth's Interior, Okayama University, Tottori, Japan.

Table 1. Average of Bulk Chemical Compositions of Argillite, After the Work of Hashimoto *et al.* [2009]

	wt%
SiO ₂	69.2
TiO ₂	0.6
Al ₂ O ₃	15.2
Fe ₂ O ₃	5.5
MnO	0.2
MgO	1.7
CaO	0.7
Na ₂ O	2.3
K ₂ O	3.6
P ₂ O ₅	0.1
H ₂ O ⁻	0.2
Total	99.3

the initial slip weakening followed by the slip strengthening up to a peak shear stress (related to the formation and coalescence of discontinuous melt patches) and finally by the secondary slip weakening toward the steady state shear stress (related to temperature-dependent melt rheology). Similar mechanical behavior was also demonstrated by HVRFE on tonalite, tonalite-derived cataclasite, and novaculite, but the transient strengthening during the formation of discontinuous melt patches was not observed in HVRFE on peridotite possibly due to very low viscosity of ultramafic melts [Di Toro *et al.*, 2006b]. The common feature of HVRFE on crystalline rocks is that slip weakening occurs once a melt layer formed and separated host rocks completely. The HVREE on crystalline rocks shows a weak dependence of steady state shear stress on melt composition [Di Toro *et al.*, 2006b], and numerical modeling incorporating the HVRFE results also indicates that shear stress drop during frictional melting is weakly dependent on melt viscosity likely due to a feedback between temperature and melt viscosity [Fialko and Khazan, 2005; Sirono *et al.*, 2006]. On the basis of HVRFE on gabbro, Hirose and Shimamoto [2005] pointed out that the physical process responsible for the slip weakening after the formation of melt layer is a decrease in shear strain rate due to the growth of melt layer. Fialko and Khazan [2005] argued that the growth of melt layer is limited by squeezing of melt from the shear zone due to normal load, and attributed the observed weakening primarily to temperature dependence of melt viscosity. The rotary friction experiments on granite at high-velocities (2.0–4.0 m/s) by Spray [2005] suggested that melt viscosity plays an important role on melt lubrication of faults: when selective melting of minerals constituting ~50% of granite (i.e., feldspar) occurred at temperatures higher than the liquidus for granite (~600°C at low pressure), low-viscosity melt can be generated owing to the high temperature (~1150°C) and the low content of SiO₂ in melt zone relative to the bulk composition of granite.

[4] In this study, we present results of HVRFE on argillite taken from the host rock of a pseudotachylyte-bearing fault in an exhumed accretionary complex. The goal of our experiments was to investigate how frictional melting of argillite affects dynamic strength of faults in subduction-accretion complexes. Microstructures and chemical composition of experimentally generated pseudotachylytes were investigated to identify the underlying physical processes

responsible for the mechanical behavior during frictional melting and then compared with those of natural pseudotachylytes in accretionary complexes exhumed from seismogenic depths. On the basis of HVRFE results and information on experimentally generated and natural pseudotachylytes, we discuss the dynamics of seismic slip in the presence of frictional melting on faults in subduction-accretion complexes.

2. Sample Preparation and Experimental Method

[5] The samples for HVRFE were collected from the argillite matrix of the tectonic mélange, which constitutes the host rock of the pseudotachylyte-bearing fault in the Late Cretaceous Shimanto accretionary complex of eastern Shikoku Island (Mugi area) in southwest Japan [Ujii *et al.*, 2007]. In the Mugi and Okitsu (western Shikoku Island) areas, pseudotachylytes were formed along the subduction thrusts or the roof thrusts of the duplex structures exhumed from seismogenic depths (4–6 km) and were derived from the frictional melting of illite-rich, argillite-derived slip zones with their thickness less than a few millimeters [Ujii *et al.*, 2007]. The argillite is foliated due to the development of pressure solution cleavage during subduction. In order to simulate in situ conditions, we selected argillite samples in which visible fragments are rare or lacking at the outcrop scale. The petrographic features and X ray diffraction patterns revealed that the major mineral constituents for argillite are quartz, feldspar, illite, and chlorite. Dominance of illite over chlorite was observed within clay minerals. Table 1 shows the bulk chemical compositions of major elements in the argillite that was analyzed using the whole-rock X-ray fluorescence method [after Hashimoto *et al.*, 2009].

[6] Experiments were conducted on a rotary shear, high-velocity frictional testing apparatus in Kyoto University [Shimamoto and Tsutsumi, 1994]. Detailed characteristics of the apparatus can be found in the works of Shimamoto and Tsutsumi [1994] and Hirose and Shimamoto [2005]. The apparatus is equipped with an air pressure driven actuator to apply an axial force (~10 kN) to a pair of solid or hollow cylindrical specimens. A 7.5 kW servo-motor rotates one of the specimens at 1500 rpm (the other specimen is kept stationary by a spline). The rotation of the motor was transmitted to the specimen through an electromagnetic clutch. The clutch was engaged within several seconds after the motor speed reached the desired value. Axial force, torque, and axial shortening of specimens were measured with a force gauge, a torque gauge, and a displacement transducer, respectively.

[7] All samples were cored perpendicular to the foliation by a motor-powered drill and were then sliced in a pair of solid cylindrical specimens (21.65 mm in diameter and ~22.67 mm in height) for each experiment. We could not prepare a pair of hollow cylindrical specimens because the coring of solid argillite cylinder resulted in destruction of specimens along the foliation. Thus all of our experiments used a pair of solid argillite cylinders with the shear direction being parallel to the foliation. In order to avoid sample destruction by thermal fracturing [Ohtomo and Shimamoto, 1994] and to achieve elevated normal stresses [Di Toro *et al.*, 2006a], specimens were jacketed with an

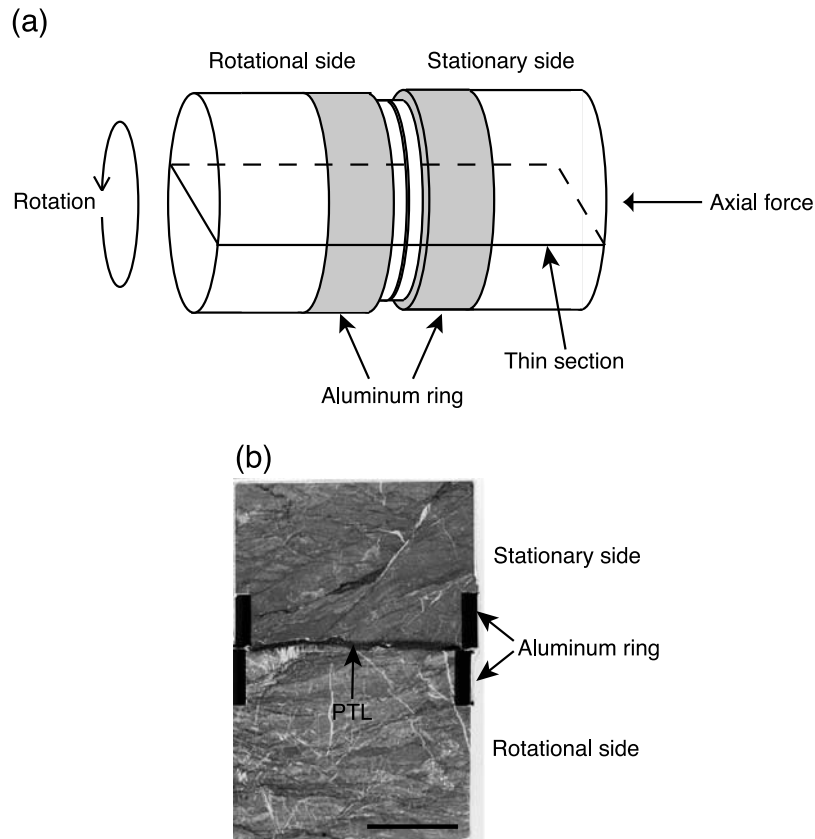


Figure 1. A specimen assembly for an HVRFE. (a) Schematic sketch showing a geometry of HVRFE. A pair of solid cylindrical specimens was jacketed with an aluminum ring. (b) A thin section of argillite samples with external aluminum ring assembly after the HVRFE. The pseudotachylyte layer (PTL) separates a pair of argillite samples and external aluminum rings. Scale bar = 10 mm.

aluminum ring (Figure 1). Each experiment was terminated before aluminum rings on the stationary and rotational sides came into contact. This was confirmed by inspections of specimens after experiments: the two opposite aluminum rings were separated by a continuous pseudotachylyte layer (Figure 1b). As described in section 3.2, the chemical analysis indicates that the pseudotachylyte layer is depleted in Al_2O_3 relative to the rocks outside the pseudotachylyte layer. Therefore the effect of the aluminum rings on experimental measurements was likely negligible.

[8] Eleven experiments were performed under dry condition at room temperature and normal stress (σ_n) of 2.67, 8.0, and 13.33 MPa. For the given configuration of a rotary shear experiment with solid cylindrical specimens, slip rate linearly varies from 0 at the center to the maximum at the boundary of the slip zone. We adopted an equivalent slip rate V_e [Shimamoto and Tsutsumi, 1994].

$$V_e = \frac{4}{3}\pi Rr \quad (1)$$

where R and r are the revolution rate of motor (1500 rpm) and the radius of the solid cylindrical specimen, respectively. V_e is defined such that V_e multiplied by the sliding surface area (S) provides the rate of frictional work, assuming constant shear stress over S . The calculated V_e is 1.13 m/s for our HVRFE. The process of frictional

melting during HVRFE was monitored using a digital video camera.

3. Results

3.1. Dynamic Shear Strength in the Postmelting Regime

[9] As we attempted to terminate experiments before the two opposite aluminum rings touched each other, the durations of experiments ranged from 3–6 s (for σ_n of 8.0 and 13.33 MPa) to 6–17 s (for σ_n of 2.67 MPa). The duration of experiments, equivalent slip rate (V_e), normal stress (σ_n), and total displacement (3–17 m) are all comparable to those of previous HVRFE on crystalline rocks. However, the evolution of shear stress during HVRFE on argillite (Figure 2a) is different from that inferred for crystalline rocks [Tsutsumi and Shimamoto, 1997; Hirose and Shimamoto, 2005; Di Toro et al., 2006b]. The shear stress initially increased up to a peak value and then decreased with displacement. During this slip weakening, wear material (powder and debris) was extruded from the slip zone; however, axial shortening was negligible. A digital video shows that during late stage of slip weakening, discontinuous, bright reddish patches began to develop along the slip zone, likely representing the growth of melt patches within the slip zone. After the slip weakening, shear stress increased with displacement until the end of the experiment. The comparison of experimental data and video

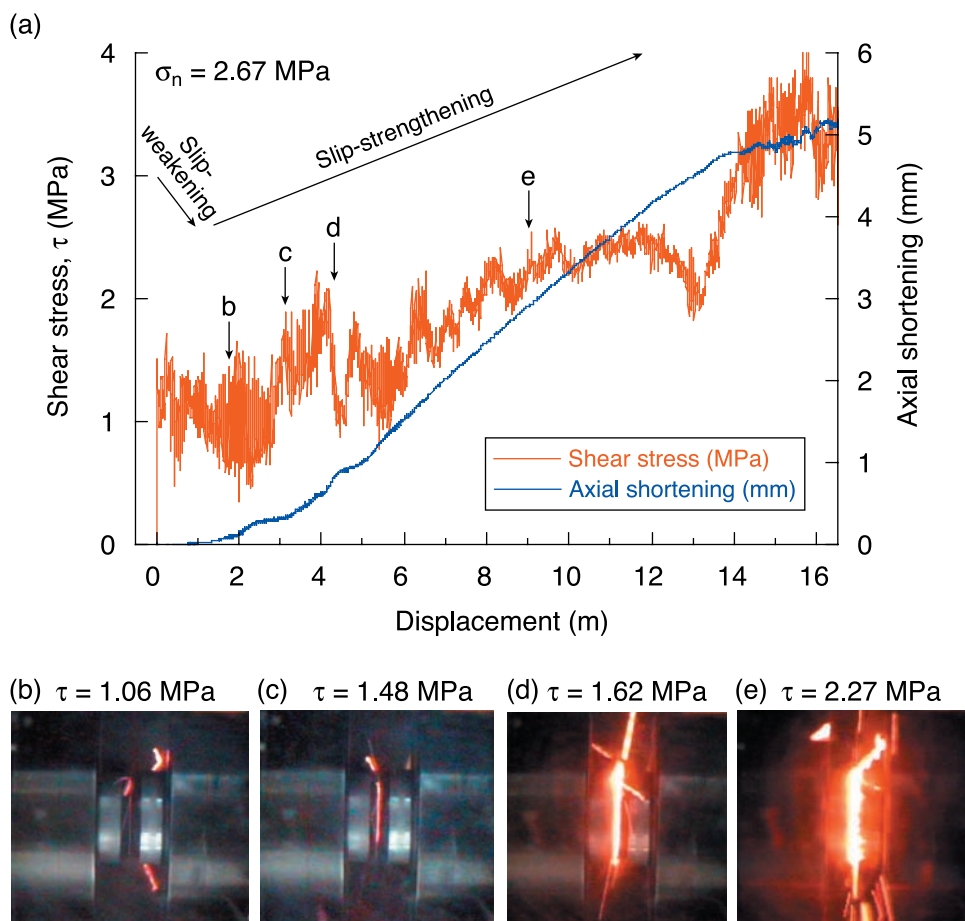


Figure 2. Experimental results for argillite at a slip rate of 1.13 m/s and σ_n of 2.67 MPa. (a) Shear stress (red line) and axial shortening (blue line) versus displacement. (b–e) Pictures captured by the digital video camera. Locations of sites are shown in Figure 2a. Note the increase in the melt layer thickness and the shear stress (τ) with displacement.

images with a time resolution of 10^{-3} s indicate that the beginning of slip strengthening corresponds to the onset of a continuous bright reddish layer. The thickness of a bright reddish layer increased during the slip strengthening, indicating a progressive growth of the melt layer (Figures 2b–2e). The latter was confirmed by visual inspection of specimens after a series of experiments with different displacements but at the same normal stress (σ_n) (see section 3.2). The onset of slip strengthening also corresponds to the onset of axial shortening (Figure 2a). The axial shortening during the strengthening stage reflects the melt squeezing due to applied normal stress and centrifugal force on the melt layer (Figures 2b–2e). In contrast to previous HVRFE on crystalline rocks, neither the slip strengthening during the formation of melt patches nor the slip weakening after the development of melt layer occurred in HVREE on argillite.

[10] As expected, the time for the bulk surface melting was shorter for larger σ_n : the melt layer was initiated after ~ 0.85 and ~ 0.43 s of slip for σ_n of 2.67 and 13.33 MPa, respectively. This is because the heat production rate during HVRFE ($\Phi \approx \mu \sigma_n V_e$, where μ is the coefficient of friction) increases with σ_n , so that the duration of slip required for the onset of melting is inversely proportional to the square

of σ_n assuming a constant coefficient of friction, constant slip rate, and a sufficiently thin slip zone [Fialko, 2004; Beeler, 2006]. Figure 3 shows an effective coefficient of friction (i.e., the ratio of shear to normal stress, τ/σ_n) measured during our HVRFE. The friction coefficient during the weakening stage was 0.2–0.5, regardless of σ_n . However, the ratio of shear to normal stress during the strengthening stage decreased with an increase in σ_n : for σ_n of 2.67, 8.0, and 13.33 MPa, the ratio of shear to normal stress was found to be 1.2–1.4, 0.8–1.0, and 0.4–0.6, respectively, at the end of the experiment (Figure 3). Since the development of a melt layer was independently confirmed during the strengthening stage, our data are suggestive of a decrease in the apparent coefficient of friction with normal stress in the postmelting regime, as predicted by theoretical models [Fialko and Khazan, 2005]. Unfortunately, the experiments were too short to confirm the postmelting steady state.

3.2. Microstructure and Chemical Composition of Experimental Shear Zones

[11] Microstructures of experimental shear zones were examined by optical microscope and scanning electron microscope. An experimental shear zone under plane-polarized light is composed of the light grayish pseudotachy-

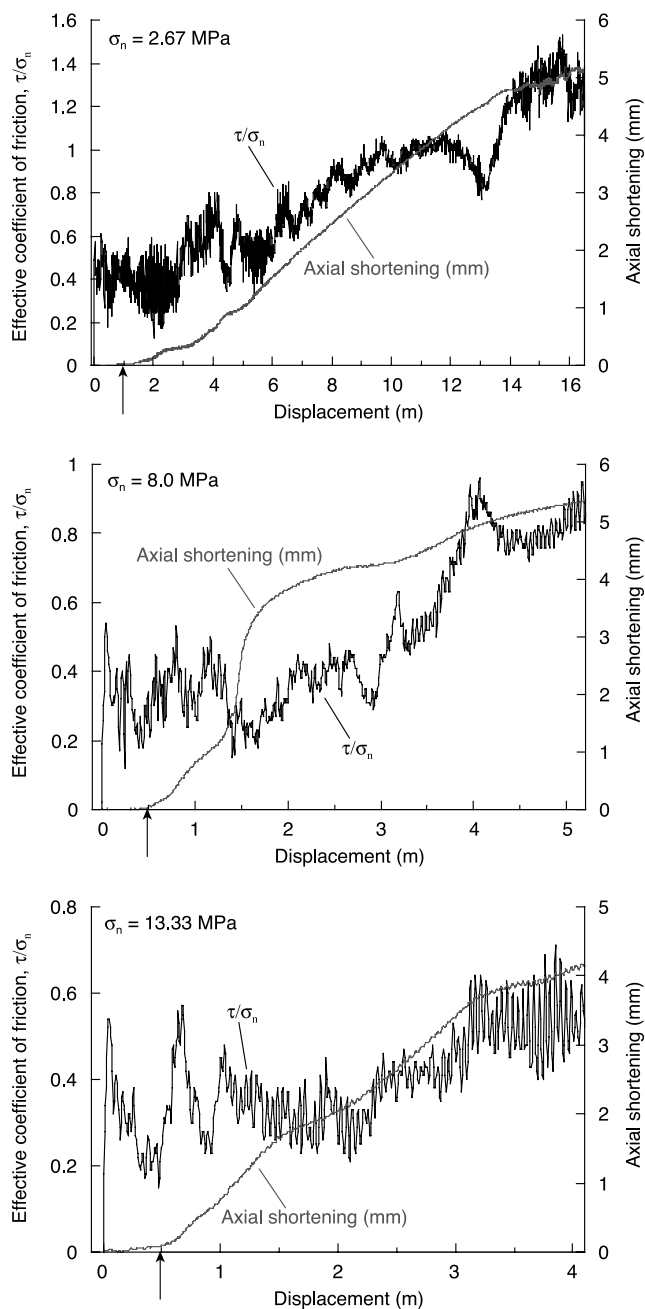


Figure 3. Effective coefficient of friction (the ratio of shear to normal stress, τ/σ_n) and axial shortening versus displacement at σ_n of 2.67, 8.0, and 13.33 MPa. The arrows denote the onset of a melt layer.

lyte layer mantled by the dark layer along both margins (Figures 4a and 4b). The thickness of pseudotachylyte and dark layers are 0.3–0.74 mm and 0.02–0.35 mm, respectively. Both pseudotachylyte and dark layers become wider with displacement; e.g., the thickness of pseudotachylyte layer increases from 0.3 to 0.57 mm when the shear displacement increased from 4.369 to 5.215 m at σ_n of 8.0 MPa (Figures 4a and 4b). Thin quartz veins are sharply cut by the pseudotachylyte layer, but the dark layers preserve these quartz veins that are inherited from the host rock (Figure 4b). This indicates that the dark layers did not accommodate any appreciable shear deformation. Under

plane-polarized light, the pseudotachylyte layer shows dominance of subangular to subrounded quartz grains over feldspar grains, which are scattered in the light grayish matrix without illite and chlorite. The dark layer is characterized by quartz and feldspar grains in the dark matrix, without clay minerals. Compared to the dark layer and the host rocks, the amount of feldspar (mainly albite) is reduced in the pseudotachylyte layer. Under cross-polarized light, the matrices of both pseudotachylyte and dark layers are dark and optically isotropic.

[12] The pseudotachylyte layer under back-scattered electron (BSE) images is characterized by the presence of quartz with minor amount of feldspar grains and spherical and ellipsoidal vesicles in the homogeneous, glassy matrix (Figures 5a–5c). In places, submicron Fe-rich bright grains are concentrated in the matrix, representing Fe-rich spherules (Figure 5b). Quartz and feldspar grains exhibit embayed and rounded margins (Figure 5c). The embayed and rounded grains as well as Fe-rich bright spots are absent in the dark layer under BSE images. However, vesicles are ubiquitously developed in the matrix of the dark layer with their size ranging from submicron to 10 μm (Figure 5d). The shape of vesicles in the dark layer is more irregular than that of vesicles in the pseudotachylyte layer.

[13] The chemical compositions of matrices of pseudotachylyte and dark layers were analyzed by an electron probe microanalyzer (JXA-8900RL) installed at the Japan Agency for Marine-Earth Science and Technology under an acceleration voltage of 15 kV with a beam current of 15 nA (the same analytical condition as that in the study of *Ujii et al.* [2007]). We used a focused beam of about 1 μm in diameter to analyze only the matrix and adopted an average of 12–27 points as a representative chemical composition. No clear spatial compositional variation was seen in both matrices of pseudotachylyte and dark layers. The EDS spectra did not detect sulfur and halide peaks. Thus an ignition loss is considered to be mostly due to evaporation of H_2O by the electron beam, which is consistent with the presence of vesicles in the matrix. The result of chemical analysis is shown in Table 2. The chemical composition of the dark layer matrix is similar to that of illite [*Deer et al.*, 1992]. The composition of the pseudotachylyte matrix is also similar to that of illite but is enriched in SiO_2 , FeO , and Na_2O and depleted in Al_2O_3 and K_2O relative to the dark layer matrix. The ignition loss of the pseudotachylyte matrix is smaller than that of the dark layer matrix, suggesting the relative depletion in H_2O .

4. Discussion

4.1. Microstructures and Chemical Composition

[14] The enrichment of SiO_2 , FeO , and Na_2O in the pseudotachylyte matrix relative to the dark layer matrix of illite composition suggests that chlorite and albite together with illite were melted during HVRFE. This is consistent with the microstructural observations, which show the absence of clasts of clay minerals in the pseudotachylyte layer, the presence of Fe-rich spherules in the pseudotachylytes, and the lower amount of albite grains in the pseudotachylyte layer with respect to the dark layer. The heating experiments on illite and the investigation of the thermal transformation of illite using X-ray diffraction, scanning

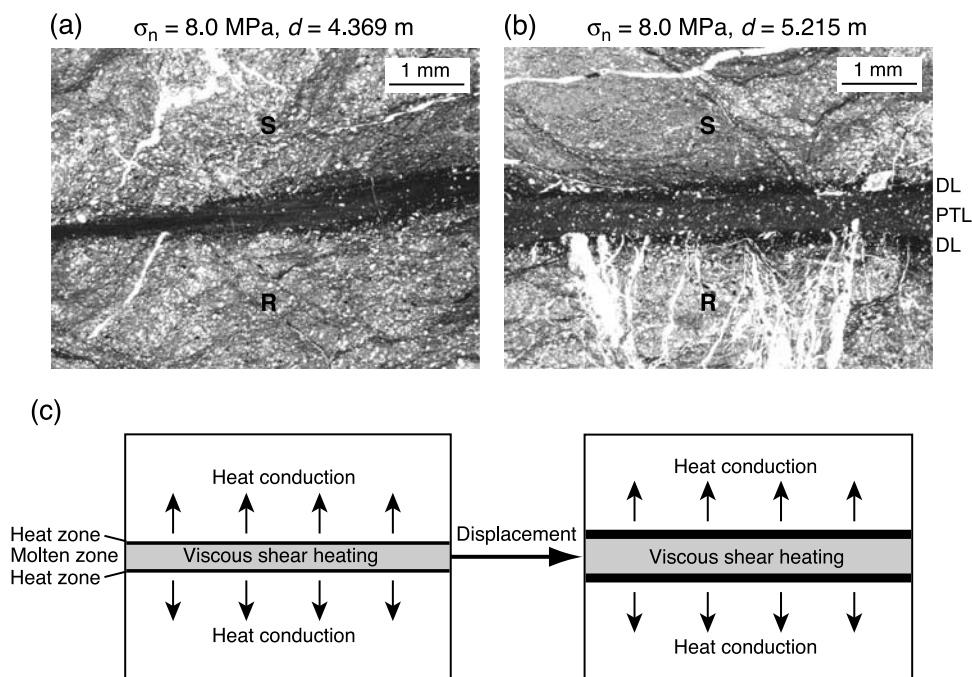


Figure 4. Microstructural evolution of an experimental shear zone. Shear zones formed at σ_n of 8.0 MPa and displacement (d) of (a) 4.369 m and (b) 5.215 m. R, rotational side; S, stationary side. Note that the quartz veins in the rotational side are sharply cut by the pseudotachylyte layer (PTL) but preserved in dark layers (DL). Plane-polarized light. (c) A schematic diagram showing an interpretation of microstructural evolution of an experimental shear zone with displacement.

electron microscope, and transmission electron microscopy reveal that illite melts at $\sim 1100\text{--}1200^\circ\text{C}$ [Grim and Bradley, 1940; McConville and Lee, 2005; Yamaguchi and Ujiie, 2005]. The surviving mineral assemblage and the melting temperature of albite [Spray, 1992] indicate the melting temperature of 1100°C . These features suggest that the pseudotachylyte layer underwent frictional melting at 1100°C and subsequent rapid cooling, resulting in a fragment-laden, glass-supported texture.

[15] The dark layers outside of the pseudotachylyte layer were not involved in shear deformation (Figure 4b). There is also no evidence of melting in the dark layer. However, the vesicles are ubiquitously present in the dark layer matrix that has the chemical composition of illite (Figure 5d and Table 2) and is optically isotropic under cross-polarized light. These features can be reproduced when the structure of illite is disrupted due to heating to $\sim 850\text{--}1000^\circ\text{C}$ [Deer et al., 1992; Shirozu, 1988; Yamaguchi and Ujiie, 2005]. We believe that the dark layers on the boundaries of the pseudotachylyte layer develop due to rapid heating by conduction from the slip interface, resulting in the development of heat zones along the margins of the molten zone (Figure 4c). The vesicles in the dark layer matrix are interpreted to result from dehydration of illite induced by viscous shear heating within the melt layer.

4.2. Initial Slip-Weakening Phase

[16] The friction coefficient varies between 0.2 and 0.5 during the initial slip weakening, regardless of σ_n . The duration of the initial slip weakening is shorter for larger σ_n , suggesting a thermally activated mechanism. The slip weakening may be attributed to flash heating at highly

stressed asperity contacts [Rice, 1999, 2006; Brown and Fialko, 2008] and/or thermal decomposition of clay minerals at subsolidus temperatures. Melt patches occurred during late stage of the slip-weakening phase. Compared to previous HVRFEs on crystalline rocks that show the marked strengthening stage associated with the formation of melt patches [Tsutsumi and Shimamoto, 1997; Hirose and Shimamoto, 2005; Di Toro et al., 2006b], melt patches in our experiments almost immediately give rise to the formation of a continuous melt layer at the beginning of the slip-strengthening phase. This remarkable difference in mechanical behavior between crystalline rocks and argillite may be due to the difference in the volume fraction of the least refractory minerals between crystalline rocks and argillite. Since selective melting of minerals commonly occurs due to the disequilibrium nature of frictional melting [Spray, 1992], incipient melt patches are presumably produced by fusion of minerals with low melting temperatures. In fact, the incipient melt patches formed during the HVFRE on gabbro are derived from biotite [Hirose and Shimamoto, 2005]. The biotite content in gabbro is very small (e.g., modal composition data indicates that biotite is less than 4% [Hirose and Shimamoto, 2005]), so that other minerals (e.g., clinopyroxene) should be melted to form a continuous melt layer. In this case, the viscosity of incipient melt patches may be high due to the low melting temperature of biotite at $\sim 650^\circ\text{C}$. The highly viscous melt patches and increases in the effective area of asperity contact due to incipient melting could cause slip strengthening during the formation of melt patches seen in HVFRE on crystalline rocks [Hirose and Shimamoto, 2005; Fialko and Khazan, 2005; Di Toro et al., 2006b]. On the other hand, the volume

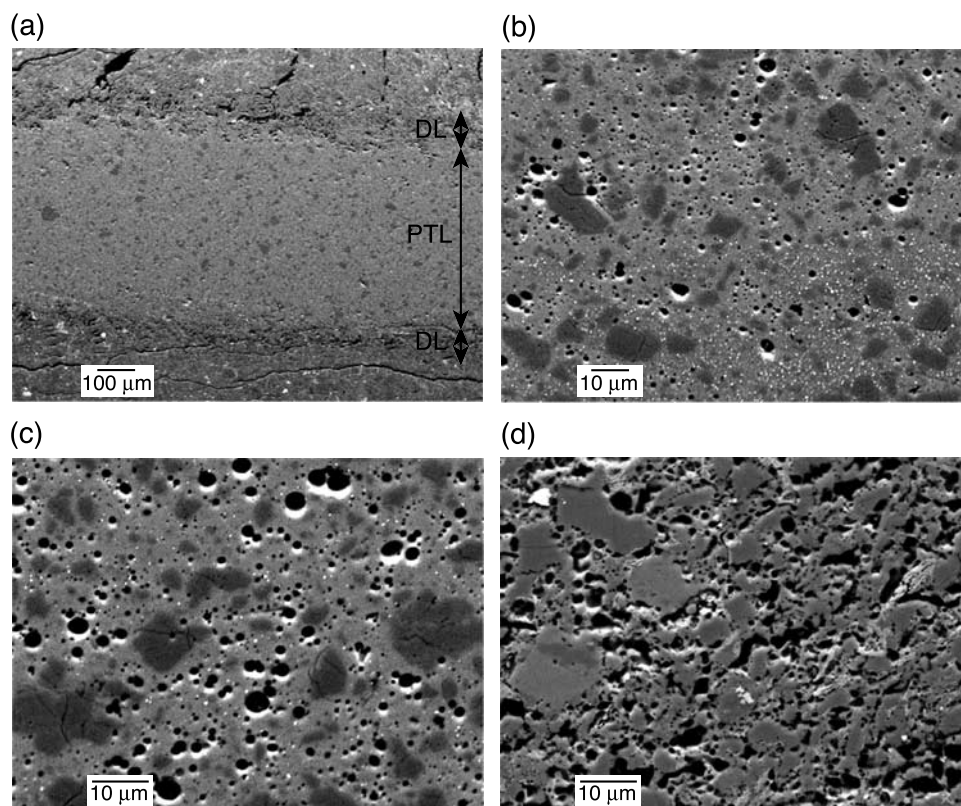


Figure 5. BSE images of an experimental shear zone. (a) A relatively bright pseudotachylyte layer (PTL) mantled by dark layers (DL) formed at σ_n of 8.0 MPa. (b) The pseudotachylyte formed at σ_n of 8.0 MPa. Fe-rich bright spots (white dots) are concentrated in the lower part. Spherical and ellipsoidal dark spots are vesicles. (c) The pseudotachylyte formed at σ_n of 2.67 MPa. Embayed and rounded grains and vesicles (spherical and ellipsoidal dark spots) are present in the homogeneous, glassy matrix. (d) The dark layer formed at σ_n of 2.67 MPa. The irregularly shaped vesicles (dark portions) develop in the matrix of illite composition (Table 2).

fraction of clay minerals (mainly illite) in argillite is 76–80% (an estimate from our 2-D measurement on thin sections). Thus once the melting temperature of the least refractory mineral is attained in argillite, the melt layer can be expected to form almost instantaneously. In this case, the transient development of melt patches in argillite is likely associated with melting of illite at high temperature ($\sim 1100^\circ\text{C}$). The slip weakening during the formation of melt patches seen in HVRFE on argillite may be due to the presence of low-viscosity melt patches.

4.3. Slip Strengthening During the Growth of Melt Layer

[17] The pseudotachylyte layer produced by HVRFE on argillite is thicker than the experimentally generated pseudotachylyte layers in crystalline rocks (e.g., 0.3–0.74 mm versus less than 0.14 mm [Hirose and Shimamoto, 2005]). Moreover, the thickness of the melt layer in argillite increases with displacement during the slip strengthening (Figure 4). Thus solid-solid contacts across the fault due to the

Table 2. Average Chemical Composition of Matrices of Pseudotachylyte and Dark Layers With Standard Deviations^a

	Pseudotachylyte Layer Matrix				Dark Layer Matrix			
	HVR1004	HVR1008	HVR1011	HVR1013	HVR1004	HVR1008	HVR1011	HVR1013
<i>n</i>	17	18	13	27	12	16	13	16
SiO ₂	60.74 ± 3.45	61.73 ± 1.05	62.57 ± 2.01	61.73 ± 3.97	61.66 ± 5.11	59.49 ± 4.21	58.71 ± 4.29	56.87 ± 3.90
TiO ₂	0.61 ± 0.09	0.76 ± 0.05	0.60 ± 0.06	0.61 ± 0.11	0.23 ± 0.15	0.37 ± 0.22	0.34 ± 0.21	0.43 ± 0.23
Al ₂ O ₃	19.30 ± 1.88	20.24 ± 0.86	19.96 ± 1.04	19.67 ± 2.07	20.38 ± 4.36	22.71 ± 4.09	22.04 ± 3.00	23.49 ± 2.66
FeO	6.31 ± 0.61	5.33 ± 0.26	4.62 ± 0.53	5.75 ± 0.78	4.08 ± 1.23	3.02 ± 0.93	3.18 ± 0.89	3.85 ± 1.57
MnO	0.28 ± 0.04	0.15 ± 0.03	0.13 ± 0.02	0.14 ± 0.02	0.14 ± 0.06	0.08 ± 0.03	0.08 ± 0.03	0.09 ± 0.04
MgO	2.59 ± 0.24	2.19 ± 0.09	2.06 ± 0.12	2.09 ± 0.31	2.08 ± 0.54	1.85 ± 0.54	1.94 ± 0.36	2.18 ± 0.49
CaO	0.91 ± 0.52	0.67 ± 0.09	0.35 ± 0.04	0.44 ± 0.15	0.15 ± 0.24	0.19 ± 0.13	0.11 ± 0.05	0.19 ± 0.28
Na ₂ O	1.90 ± 0.38	1.89 ± 0.41	2.27 ± 0.24	1.92 ± 0.26	1.64 ± 0.79	1.85 ± 0.87	1.78 ± 1.07	1.49 ± 0.79
K ₂ O	4.80 ± 0.48	4.53 ± 0.22	4.54 ± 0.22	4.26 ± 0.52	6.26 ± 1.71	6.73 ± 1.38	6.70 ± 1.30	7.02 ± 1.21
Total	97.44	97.5	97.10	96.61	96.61	96.28	94.88	95.61
Ignition loss	2.56	2.5	2.9	3.39	3.39	3.72	5.12	4.39

^a*n*, numbers of analyses.

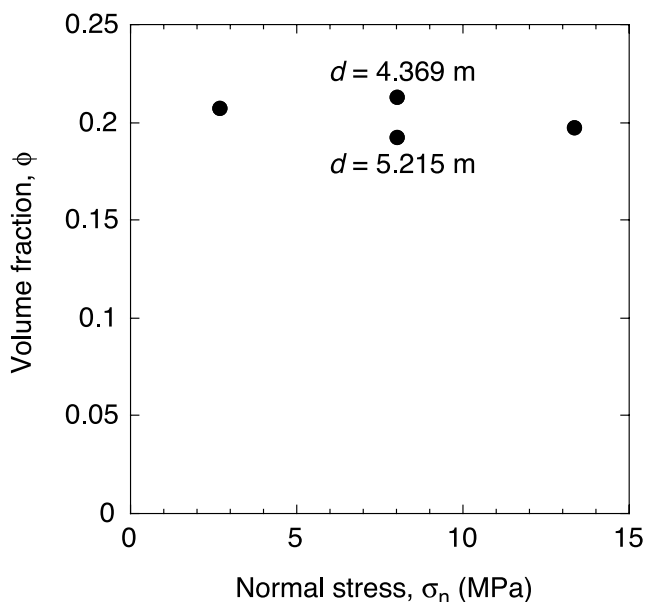


Figure 6. Averaged volume fraction (ϕ) of solid grains in the pseudotachylyte plotted against normal stress (σ_n). Standard deviations are smaller than the solid circle size. d , displacement.

thinning of melt layer [Tsutsumi and Mizoguchi, 2007] are unlikely to occur. When the host rocks are completely separated by the melt layer, and the slip rate (V) is constant, the viscous shear stress (τ) obeys the lubrication approximation.

$$\tau = \eta \frac{d\gamma}{dt} = \eta \frac{V}{w} \quad (2)$$

where η is the effective viscosity of the melt layer, $d\gamma/dt$ is the shear strain rate, and w is the thickness of the melt layer. During the slip strengthening, the shear strain rate is decreased due to an increase in w . For example, when shear displacement increases from 4.4 to 5.2 m, the ratio V/w is found to decrease by a factor of 0.66 because w increases from 0.45 to 0.69 mm (Figures 4a and 4b). At the same time, the experimental data indicate that τ is increased by a factor of 1.25. This observation suggests that the slip strengthening is attributed to an increase in the effective melt viscosity.

[18] The factors controlling an increase in the viscosity of the melt layer during the slip strengthening include (1) increases in volume fraction of solid grains and/or bubbles in the melt layer and (2) increases in the matrix viscosity of the melt layer. The viscosity of a suspension is affected by the volume fraction of solid grains and bubbles [e.g., Metzner, 1985; Kraynik, 1988; Spray, 1993]. The relative viscosity (η_r , the ratio of the viscosity with solid grains to the inclusion-free fluid viscosity) can be described using an empirical equation [Kitano *et al.*, 1981].

$$\eta_r = \left[1 - \left(\frac{\phi}{A} \right) \right]^{-2} \quad (3)$$

with $A = 0.54 - 0.0125r$, where ϕ is the volume fraction of the solid grains, A is the parameter related to the packing

geometry of the solid grains, and r is the average aspect ratio of the solid grains. We estimated ϕ in the pseudotachylyte layer using BSE images with a 1500-fold magnification. We measured ϕ at the center, the margin, and the halfway point of the pseudotachylyte layer and then averaged the values. ϕ in the pseudotachylyte layer is small ranging 0.19–0.21, regardless of σ_n (Figure 6). This indicates that the volume fraction of the solid grains in the pseudotachylyte layer is nearly the same as that of grains other than clay minerals in the host rock (0.2–0.24). If we compare ϕ in the pseudotachylyte layers formed at the same σ_n but different displacements (d), ϕ slightly decreases with displacement (Figure 6). Therefore the viscosity increase due to the increase in the volume fraction of solid grains in the melt layer is unlikely to occur during the slip strengthening. We also estimated the volume fraction of vesicles in the pseudotachylyte layer using the same procedure as in the case of solid grains. The volume fraction of vesicles was found to be less than 0.05. Given the very small volume fraction of vesicles, the contribution of bubbles to the viscosity increase in the melt layer is negligible.

[19] Microstructural and chemical analyses suggest that the dark layer is eventually incorporated into the melt layer (Figure 4) and that dehydration is stronger in the melt layer than in the dark layer (Table 2). We postulate that the chemical composition of the melt layer matrix at the beginning of slip strengthening (i.e., at the onset of macroscopic melting) preserves the composition of the dark layer matrix (i.e., illite composition) and then changes to the composition of the pseudotachylyte layer matrix (i.e., enriched in SiO_2 , FeO , and Na_2O and depleted in Al_2O_3 , K_2O , and H_2O) as slip proceeds. The assumption of the initial melt layer having illite composition is supported by the fact that the chemical composition of argillite-derived natural pseudotachylytes closely resembles that of illite [Ujii *et al.*, 2007]. Figure 7 shows shear stress and axial shortening versus displacement in the HVRFE at σ_n of 13.33 MPa. The onset of melting is coincident with the onset of axial shortening associated with the melt extrusion (see arrow in Figure 7). We calculated the matrix (not including grains and vesicles) viscosity of the melt layer at the beginning of the strengthening stage using the chemical composition of the dark layer matrix (HVR1008 in Table 2). The calculation considers the Arrhenian temperature dependence of melt viscosity.

$$\eta(T) = A \exp\left(\frac{B}{T}\right) \quad (4)$$

where T is the absolute temperature, and A and B are the reference viscosity (temperature-independent prefactor) and the activation temperature, respectively [e.g., Fialko and Khazan, 2005]. Theoretical arguments and experimental data suggest that equation (4) is adequate for most silicate melts [e.g., Shaw, 1972; Dingwell, 1998]. In addition, recent modeling studies indicate that hydrous melts tend to be more Arrhenian-like than anhydrous melts over large temperature intervals [Giordano *et al.*, 2008]. If we adopt the melting temperature of illite of 1100°C, then the matrix viscosity of the melt layer at the beginning of slip strengthening is 416 Pa s (Figure 8). We take the chemical

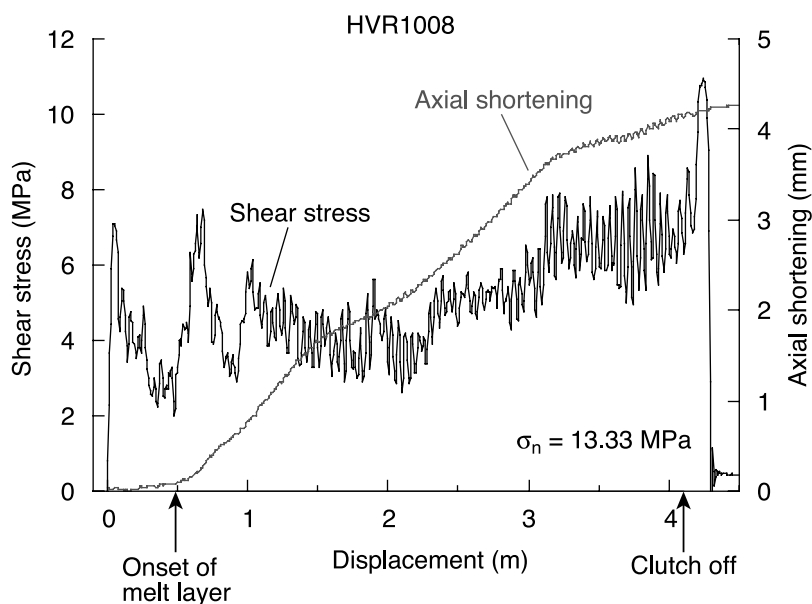


Figure 7. Experimental results at σ_n of 13.33 MPa (HVR1008) showing shear stress (black line) and axial shortening (dark gray line) versus displacement. An increase in shear stress after the disengagement of the clutch reflects that slip due to inertia occurs along the rapidly cooling melt layer.

composition of the pseudotachylyte layer matrix at the end of the experimental run as representative of the composition of the melt layer matrix during the experiment (arrow in Figure 7). This is because once the clutch is disengaged at the end of the HVRFE, the melt layer rapidly solidifies due to cooling, and slip is abruptly terminated. The chemical composition and microstructural features of the pseudotachylyte layer indicate the melting of albite at 1100°C, so that the increase in the matrix viscosity due to a decrease in temperature is unlikely to occur during the strengthening

stage. At the end of the experiment (i.e., the disengagement of the clutch), the matrix viscosity and the viscosity of the melt layer (corrected for clast content using equation (3)) at 1100°C are $1.5 \cdot 10^3$ and $4 \cdot 10^3$ Pa s, respectively (Figure 8). The estimated viscosity of the melt layer (solid square in Figure 8) is close to the apparent viscosity (solid diamond in Figure 8) determined by dividing the measured shear stress by the shear strain rate. Since the change in volume fraction of solid grains is negligible during frictional melting, the change in the viscosity of the melt layer during the slip

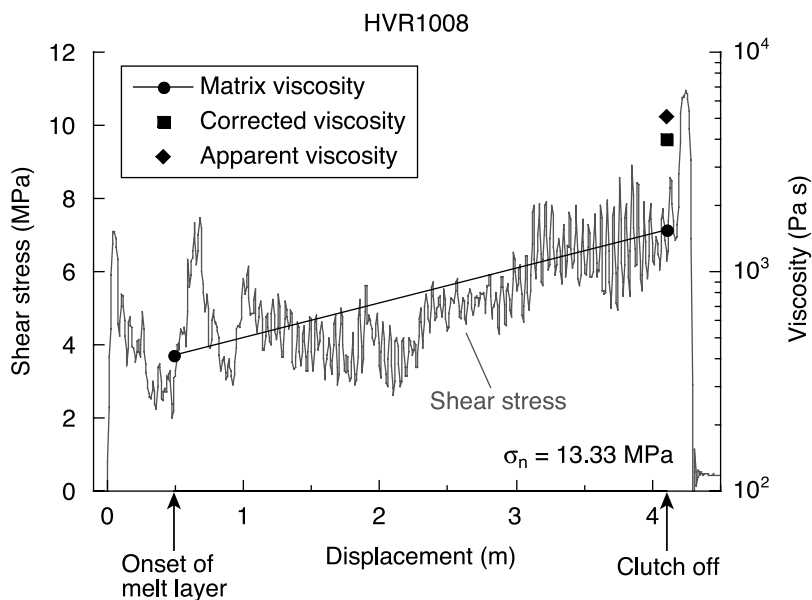


Figure 8. Plots of the matrix viscosity (solid circles), the viscosity of the melt layer (solid square), and the apparent viscosity (solid diamond). The shear stress versus displacement shown in Figure 7 is also presented for comparison.

strengthening can be evaluated from the change in the matrix viscosity from the beginning to the end of the strengthening phase; the viscosity increases by a factor of 3.69. The experimental data show that the shear stress increases by a factor of 2.25 during the slip strengthening. Some of this difference is compensated by a decrease in shear strain rate associated with the growth of melt layer (Figures 4a and 4b).

[20] On the basis of the viscosity calculation using chemical composition data in Table 2, an increase in the matrix viscosity during the slip strengthening is mainly due to the reduction in H₂O content with lesser contribution of a slight increase in SiO₂ content. An appreciable dehydration of the melt layer is not surprising in the HVRFE on argillite, because of the abundance of hydrous clay minerals (76–80%), and the unconfined environment, so that volatiles can escape along with the melt due to extrusion in a radial direction. Indeed, the release of H₂O is evidenced by the presence of vesicles in the pseudotachylyte (Figures 5a–5c). Strengthening in the postmelting regime has not been observed in HVRFE on crystalline rocks; however, it was recently reported in the HVRFE on metamorphosed siltstone (illite was transformed to muscovite) [Kim *et al.*, 2008] and argillite-dominated tectonic mélange collected near the pseudotachylyte-bearing fault in the Kodiak accretionary complex in Alaska [Tsutsumi *et al.*, 2008]. Strengthening due to dehydration of the melt layer may be specific to argillite, which has abundant hydrous clay minerals (e.g., illite) that are unstable at high temperature. Additional HVRFE on various types of argillaceous rocks will be necessary to test this hypothesis.

5. Implications for Seismic Slip in Subduction-Acretion Complexes

[21] The apparent coefficient of friction along the argillite-derived melt layer is 1.2–1.4 for normal stress of 2.67 MPa and 0.8–1.0 for normal stress of 8.0 MPa (Figure 3). These values are higher than the friction coefficient of illite gouge or illite-dominated argillite ($\mu_i = \sim 0.25\text{--}0.68$) [e.g., Morrow *et al.*, 1992; Saffer and Marone, 2003; Brown *et al.*, 2003; Marone *et al.*, 2005]. The duration of the HVRFE at σ_n of 8.0 is 3–6 s, which is comparable to the rise time of large earthquakes [Heaton, 1990; Scholz, 2002]. Thus frictional melting might inhibit seismic slip in the shallow part of subduction-accretion complexes. Such viscous braking may lead to slip transfer to a new plane [e.g., Fialko, 2004].

[22] On the other hand, the ratio of viscous shear stress to fault-normal stress σ_n during the melting-induced slip strengthening is expected to decrease with an increase in σ_n . In particular, the apparent coefficient of friction is 0.4–0.6 when σ_n is 13.33 MPa (Figure 3). Assuming that the maximum values of shear stress recorded at the end of our experimental runs are close to steady state values, our experimental data are consistent with theoretical predictions of a weak (if any) dependence of viscous stress on σ_n [e.g., Fialko and Khazan, 2005]. This implies that even if dehydration of the melt layer occurs on a timescale of seismic slip, the ratio of viscous shear stress to σ_n may decrease with depth. Thus there could be a critical depth below which the ratio of viscous shear stress to σ_n is less

than the friction coefficient of illite gouge or illite-dominated argillite.

$$\frac{\eta}{\sigma_n} \frac{d\gamma}{dt} < \mu_i. \quad (5)$$

Below the critical depth, melt lubrication is likely to occur, resulting in nearly complete stress drops and increased seismic efficiency.

[23] The HVRFE on argillite successfully reproduced the microstructures of natural pseudotachylytes in exhumed accretionary complexes; both natural and experimentally generated pseudotachylytes display a fragment-laden, glass-supported texture (Figures 5a–5c). However, dark layers formed by heat conduction from the melt layer are absent around illite-rich, argillite-derived natural pseudotachylyte layers formed at seismogenic depths of 4–6 km [Ujii *et al.*, 2007]. On the other hand, the chemical composition of these natural pseudotachylytes is closer to that of the experimentally produced dark layers, than to the chemical composition of experimentally produced pseudotachylyte layers [Ujii *et al.*, 2007] (Table 2). At the same time, the H₂O content of natural pseudotachylytes estimated from an ignition loss is higher than the H₂O content in experimentally produced dark layers. The experimental procedure (in particular, analytical condition and electron probe microanalyzer) was identical for measuring the chemical composition of experimentally generated dark and pseudotachylyte layers and argillite-derived natural pseudotachylytes. Therefore it appears that natural pseudotachylytes lack evidence for thermal erosion of the host rocks associated with progressive widening of the melt layer and are more hydrous than the experimentally generated pseudotachylytes. The absence of a dark layer and the water-enriched composition of natural pseudotachylytes in the exhumed subduction thrusts are likely indicative of hydrous conditions at seismogenic depth. Additional factors bearing on the reported differences between experimental and natural pseudotachylytes include lower in situ permeabilities of host rocks and shorter earthquake slip durations compared to the duration of the HVRFE (3–17 s), both of which would act to reduce volatile loss and dehydration. If so, dark layers are unlikely to form next to pseudotachylyte layers at seismogenic depths, and the thickness of natural pseudotachylyte layers may be viewed as a direct proxy for the effective thickness of the seismic slip zone (after appropriate corrections for the melt loss due to injection). Hydrous melts at seismogenic depths can possibly contribute to melt lubrication of faults during earthquakes in subduction-accretionary complexes, e.g., the viscosities at 1100°C estimated from natural pseudotachylytes [Ujii *et al.*, 2007] are one or two orders of magnitude lower than those of experimentally generated pseudotachylytes.

6. Conclusions

[24] We conducted high-velocity friction experiments at a slip rate of 1.13 m/s and normal stress σ_n of 2.67–13.33 MPa. Experiments were conducted on argillite that is a common fault zone material for pseudotachylyte-bearing faults in accretionary complexes exhumed from seismogenic depths. Our experimental results are markedly different from those

reported for crystalline rocks. In particular, we observe slip weakening followed by the slip strengthening in the course of individual experiments. During the slip-weakening phase, discontinuous melt patches formed at high temperature ($\sim 1100^{\circ}\text{C}$). The development of melt patches is transient and immediately followed by a formation of a continuous melt layer, most likely due to a high content of least refractory minerals (illite). The formation and shearing of low-viscosity melt patches as well as flash heating and thermal decomposition of clay minerals could contribute to the slip weakening. The subsequent slip strengthening corresponds to the viscous shear of a continuous film of melt. During the strengthening phase, the shear strain rate decreases in association with a progressive widening of the melt layer, implying an increase in the effective viscosity of the frictionally generated melt. The viscosity increase during the slip strengthening is most likely due to dehydration of the melt layer and the adjacent solid (the “dark layer”) that may be subsequently incorporated in the melt layer by thermal erosion. Such dehydration may be specific to clay mineral (illite)-dominated argillite. Our experimental results imply that the frictional melting at shallow depths in subduction-accretion complexes may lead to suppression of seismic slip due to viscous braking if a substantial melt dehydration occurs on a timescale of seismic slip. On the other hand, our experimental data also suggest that the ratio of viscous shear stress to σ_n progressively decreases with depth, and may eventually become less than the friction coefficient of the fault zone material at greater depths. Compared to experimentally generated pseudotachylytes, argillite-derived natural pseudotachylytes formed at seismogenic depths within subduction-accretion complexes are more hydrous, presumably due to water-saturated environment, relatively impervious fault zone rocks, and longer slip duration in our experiments compared to the typical earthquake rise times. Experimental data combined with field observations suggest that viscous braking could be possible at shallow depths, while melt lubrication is more likely at greater depths; a transition from melt lubrication to viscous braking may be one of the factors controlling the updip limit of the seismogenic zone in subduction-accretion complexes.

[25] **Acknowledgments.** This research was funded by the Grant-in-Aid for Scientific Research, Japan Society for Promotion of Science (17340152) and Japan Agency for Marine-Earth Science and Technology. We thank J.G. Spray and J.C. Moore for suggestions and improvements. We also thank T. Kozono for useful discussions.

References

- Beeler, N. M. (2006), Inferring earthquake source properties from laboratory observations and the scope of lab contributions to source physics, in *Radiated Energy and the Physics of Earthquake Faulting*, *Geophys. Monogr. Ser.*, vol. 170, edited by R. Abercrombie et al., pp. 99–119, AGU, Washington, D. C.
- Brown, K., and Y. Fialko (2008), Friction at seismic slip speeds: Experiments and theory, *Eos Trans. AGU*, 89(53), Fall Meet. Suppl., Abstract T21D-05.
- Brown, K. M., A. Kopf, M. B. Underwood, and J. L. Weinberger (2003), Compositional and fluid pressure controls on the state of stress on the Nankai subduction thrust: A weak plate boundary, *Earth Planet. Sci. Lett.*, 214, 589–603.
- Deer, W. A., R. A. Howie, and J. Zussman (1992), *An Introduction to the Rock-Forming Minerals*, 2nd ed., 696 pp., Longmans, London, U. K.
- Dingwell, D. (1998), Melt viscosity and diffusion under elevated pressures, *Rev. Miner.*, 37, 397–424.
- Di Toro, G., T. Hirose, S. Nielsen, G. Pennacchioni, and T. Shimamoto (2006a), Natural and experimental evidence of melt lubrication of faults during earthquakes, *Science*, 311, 647–649.
- Di Toro, G., T. Hirose, S. Nielsen, and T. Shimamoto (2006b), Relating high-velocity rock-friction experiments to coseismic slip in the presence of melts, in *Radiated Energy and the Physics of Earthquake Faulting*, *Geophys. Monogr. Ser.*, vol. 170, edited by R. Abercrombie et al., pp. 121–134, AGU, Washington, D. C.
- Fialko, Y. (2004), Temperature fields generated by the elastodynamic propagation of shear cracks in the Earth, *J. Geophys. Res.*, 109, B01303, doi:10.1029/2003JB002497.
- Fialko, Y., and Y. Khazan (2005), Fusion by earthquake faulting: Stick or slip?, *J. Geophys. Res.*, 110, B12407, doi:10.1029/2005JB003869.
- Giordano, D., J. K. Russell, and D. B. Dingwell (2008), Viscosity of magmatic liquids: A model, *Earth Planet. Sci. Lett.*, 271, 123–134.
- Grim, R. E., and W. F. Bradley (1940), Investigation of the effect of heat on the clay minerals illite and montmorillonite, *J. Am. Ceram. Soc.*, 23, 242–248.
- Hashimoto, Y., A. Nikaizo, and G. Kimura (2009), A geochemical estimation of fluid flux and permeability for a fault zone in Mugé mélange, the Cretaceous Shimanto Belt, SW Japan, *J. Struct. Geol.*, 31, 208–214.
- Heaton, T. H. (1990), Evidence for and implications of self healing pulses of slip in earthquake rupture, *Phys. Earth Planet. Inter.*, 64, 1–20.
- Hirose, T., and T. Shimamoto (2005), Growth of molten zone as a mechanism of slip weakening of simulated faults in gabbro during frictional melting, *J. Geophys. Res.*, 110, B05202, doi:10.1029/2004JB003207.
- Ikesawa, E., A. Sakaguchi, and G. Kimura (2003), Pseudotachylyte from an ancient accretionary complex: Evidence for melt generation during seismic slip along master décollement?, *Geology*, 31, 637–640.
- Kame, N., J. R. Rice, and R. Dmowska (2003), Effects of prestress state and rupture velocity on dynamic fault branching, *J. Geophys. Res.*, 108(B5), 2265, doi:10.1029/2002JB002189.
- Kim, J., J. Ree, R. Han, and T. Shimamoto (2008), Frictional melt: Fault lubrication or brake?, *Eos Trans. AGU*, 89(53), Fall Meet. Suppl., Abstract T13A-1921.
- Kitano, T., T. Kataoka, and T. Shirota (1981), An empirical equation of the relative viscosity of polymer melts filled with various inorganic fillers, *Rheol. Acta*, 20, 207–209.
- Kraynik, A. M. (1988), Foam flows, *Annu. Rev. Fluid Mech.*, 20, 325–357.
- Marone, C., D. Saffer, A. McKiernan, C. Rowe, and J. Samuelsen (2005), Friction constitutive properties of fault zone materials, *Eos Trans. AGU*, 86(52), Fall Meet. Suppl., Abstract S32B-05.
- McConville, C. J., and W. E. Lee (2005), Microstructural development on firing illite and smectite clays compared with that in kaolinite, *J. Am. Ceram. Soc.*, 88, 2267–2276.
- Metzner, A. B. (1985), Rheology of suspensions in polymeric liquids, *J. Rheol.*, 29, 739–775.
- Moore, G. F., N. L. Bangs, A. Taira, S. Kuramoto, E. Pangborn, and H. J. Tobin (2007), Three-dimensional splay fault geometry and implications for tsunami generation, *Science*, 318, 1128–1131.
- Morrow, C., B. Radney, and J. D. Byerlee (1992), Frictional strength and the effective pressure law of monmorillonite and illite clays, in *Fault Mechanics and Transport Properties of Rocks; A Festschrift in Honor of W. F. Brace*, edited by B. Evans, pp. 69–88, Elsevier, New York.
- Mukoyoshi, H., A. Sakaguchi, K. Otsuki, T. Hirono, and W. Soh (2006), Co-seismic frictional melting along an out-of-sequence thrust in the Shimanto accretionary complex: Implications on the tsunamigenic potential of splay faults in modern subduction zones, *Earth Planet. Sci. Lett.*, 245, 330–343.
- Nielsen, S., G. Di Toro, T. Hirose, and T. Shimamoto (2008), Frictional melt and seismic slip, *J. Geophys. Res.*, 113, B01308, doi:10.1029/2007JB005122.
- Ohtomo, Y., and T. Shimamoto (1994), Significance of thermal fracturing in the generation of fault gouge during rapid fault motion: An experimental verification (in Japanese with English abstract), *Struct. Geol.*, 39, 135–144.
- Okamoto, S., G. Kimura, S. Takizawa, and H. Yamaguchi (2006), Earthquake fault rock indicating a coupled lubrication mechanism, *eEarth*, 1, 23–28.
- Pacheco, J. F., L. R. Sykes, and C. H. Scholz (1993), Nature of seismic coupling along simple plate boundaries of the subduction type, *J. Geophys. Res.*, 98, 14,133–14,159.
- Park, J., T. Tsuru, S. Kodaira, P. R. Cummins, and Y. Kaneda (2002), Splay fault branching along the Nankai subduction zone, *Science*, 297, 1157–1160.
- Rice, J. R. (1999), Flash heating at asperity contacts and rate-dependent friction, *Eos Trans. AGU*, 80, 46 pp., Fall Meet. Suppl., Abstract F6811.
- Rice, J. R. (2006), Heating and weakening of faults during earthquake slip, *J. Geophys. Res.*, 111, B05311, doi:10.1029/2005JB004006.

- Rowe, C. D., J. C. Moore, F. Meneghini, and A. W. McKiernan (2005), Large-scale pseudotachylytes and fluidized cataclasites from an ancient subduction thrust fault, *Geology*, *33*, 937–940.
- Saffer, D. M., and C. Marone (2003), Comparison of smectite- and illite-rich gouge frictional properties: Application to the updip limit of the seismogenic zone along subduction megathrusts, *Earth Planet. Sci. Lett.*, *215*, 219–235.
- Scholz, C. H. (2002), *The Mechanics of Earthquakes and Faulting*, 2nd ed., Cambridge Univ. Press, New York.
- Shaw, H. R. (1972), Viscosities of magmatic silicate liquids: An empirical method of prediction, *Am. J. Sci.*, *272*, 870–893.
- Shimamoto, T., and A. Tsutsumi (1994), A new rotary-shear high-velocity frictional testing machine: Its basic design and scope of research (in Japanese with English abstract), *Struct. Geol.*, *39*, 65–78.
- Shirozu, H. (1988), *Introduction to Clay Mineralogy: Fundamentals for Clay Science* (in Japanese), 185 pp., Asakura Printing Co-Ltd., Tokyo.
- Sirono, S., K. Satomi, and S. Watanabe (2006), Numerical simulations of frictional melting: Small dependence of shear stress drop on viscosity parameters, *J. Geophys. Res.*, *111*, B06309, doi:10.1029/2005JB003858.
- Spray, J. G. (1992), A physical basis for the frictional melting of some rock-forming minerals, *Tectonophysics*, *204*, 205–221.
- Spray, J. G. (1993), Viscosity determinations of some frictionally generated silicate melts: Implications for fault zone rheology at high strain rates, *J. Geophys. Res.*, *98*, 8053–8068.
- Spray, J. G. (2005), Evidence for melt lubrication during large earthquakes, *Geophys. Res. Lett.*, *32*, L07301, doi:10.1029/2004GL022293.
- Tsutsumi, A., and T. Shimamoto (1997), High-velocity frictional properties of gabbro, *Geophys. Res. Lett.*, *24*, 699–702.
- Tsutsumi, A., and K. Mizoguchi (2007), Effect of melt squeezing rate on shear stress along a simulated fault in gabbro during frictional melting, *Geophys. Res. Lett.*, *34*, L21306, doi:10.1029/2007GL031565.
- Tsutsumi, A., C. D. Rowe, J. C. Moore, F. Meneghini, and A. Yamaguchi (2008), High velocity frictional properties of subducting materials: An example study for argillaceous mélange rock, paper J163-002 presented at the Japan Geoscience Union Meeting 2008, Chiba, Japan.
- Ujii, K., H. Yamaguchi, A. Sakaguchi, and S. Toh (2007), Pseudotachylytes in an ancient accretionary complex and implications for melt lubrication during subduction zone earthquakes, *J. Struct. Geol.*, *29*, 599–613.
- Yamaguchi, H., and K. Ujii (2005), Short time heating and cooling experiment on illite, *Eos Trans. AGU*, *86*(52), Fall Meet. Suppl., Abstract T21B-0480.

Y. Fialko, Institute of Geophysics and Planetary Physics, Scripps Institution of Oceanography, University of California, San Diego, Munk Building, La Jolla, CA 92093, USA.

A. Tsutsumi, Department of Geology and Mineralogy, Division of Earth and Planetary Sciences, Graduate School of Science, Kyoto University, Kyoto 606-8502, Japan.

K. Ujii, Institute for Research on Earth Evolution, Japan Agency for Marine-Earth Science and Technology, 3173-25 Showa-machi, Kanazawa-ku, Yokohama, Kanagawa 236-0001, Japan. (ujii@jamstec.go.jp)

H. Yamaguchi, Institute for Study of the Earth's Interior, Okayama University, 827 Yamada, Misasa, Tottori 682-0193, Japan.